1995 American Control Conference

Vibration Reduction Using Multi-Hump Extra-Insensitive Input Shapers

William E. Singhose
Dept. of Mechanical Engineering
Massachusetts Institute of Technology
Cambridge, MA

Lisa J. Porter
Dept. of Nuclear Engineering
Massachusetts Institute of Technology
Cambridge, MA

Neil C. Singer
Convolve, Inc.
Armonk, NY

Abstract

Input shaping is a method for reducing residual vibrations in computer controlled machines. Vibration is eliminated by convolving an input shaper, which is a sequence of impulses, with a desired system command to produce a shaped input. The shaped input then becomes the command to the system. Requiring the vibration reduction to be insensitive to modeling errors and system nonlinearities is critical to the success of the shaping process on any real system. Input shapers can be made very insensitive to parameter uncertainty; however, increasing insensitivity usually increases system delays. A design process is presented that generates input shapers with insensitivity-to-time-delay ratios that are much larger than traditionally designed input shapers. The advantages of the new shapers are demonstrated with simulations of a simple linear system and simulations of the MACE experimental apparatus.

Introduction

Input shaping is a method of reducing residual vibrations in computer controlled machines. The method requires only a simple system model consisting of estimates of the natural frequencies and damping ratios. Input shaping is implemented by convolving an input shaper, which is made up of a sequence of impulses, with a desired system command to produce a shaped input that is then used to command the system.

The convolution process lengthens the command signal by an amount equal to the time duration of the input shaper. Therefore, it is desirable to make the input shaper as short as possible, so that system delays are minimized. However, traditional design methods require that the input shaper be lengthened if additional insensitivity to modeling errors is required. This paper will present an algorithm for increasing insensitivity without increasing shaper length.

During its original presentation [13, 14], input shaping was explained by a variety of methods, including time domain analysis, vector diagram representation, frequency domain analysis, phase plane description, and pole-zero cancellation in the s-plane. The vector diagram was used to improve insensitivity [18] and cancel multiple modes of vibration [15]. The frequency domain and pole-zero cancellation representations have been investigated in several papers [2, 8, 10, 12, 16, 21].

Input shaping was shown to reduce residual vibration and maximum deflections during the slewing of a large nonlinear space-based antenna [1] and long-reach manipulators [7, 10]. Two-mode input shapers were used to increase the throughput of a silicon wafer handling robot [11]. Input shaping has been extended to systems equipped only with constant-amplitude actuators [9, 16, 17, 23]. Trajectory-following applications have also been shown to benefit from input shaping [4, 19].

A brief review of input shaping will be given in the next section. The new input shapers are then designed and their vibration-reducing properties are explained in the s-plane. Computer simulations are then used to demonstrate the advantages of the new shapers. Conclusions will be presented in the final section.

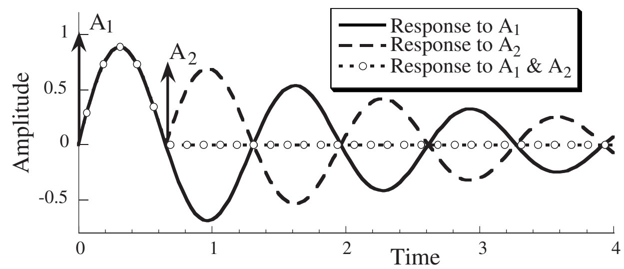

Figure 1: Vibration Cancellation Using Two Impulses.

Review of Input Shaping

For more information than this brief review, see [13, 14, 18]. Input shaping reduces residual vibration by generating an input that cancels its own vibration. The simplest self-canceling input consists of two impulses. The first impulse, which starts the system vibrating, is located at time zero, and the second impulse is delayed by one half period of the system vibration. The vibration caused by the second impulse is out of phase with the first vibration, thereby canceling it. This result is demonstrated in Figure 1. Because impulses cannot be used to move real systems, the two impulses, also known as the input shaper, must be convolved with a physically realizable input. The shaped input that results from the convolution will have the same vibration-canceling properties as the input shaper [14].

The second impulse must have the proper amplitude if it is to cancel the vibration from the first impulse. The amplitude can be determined by forming an expression for the residual vibration and then setting the expression equal to zero. The residual vibration amplitude can be expressed as the ratio of residual vibration with shaping to that without shaping. This percentage vibration can be determined by using the expression for residual vibration of a second-order harmonic oscillator of frequency ω radians/sec and damping ratio ζ, which is given in [3]. The vibration from a series of impulses is divided by the vibration from a single impulse to get the percentage vibration:

$$V(\omega)=e^{-\zeta\omega t_n}\sqrt{\left(\sum_{i=1}^{n}A_i e^{\zeta\omega t_i}\cos(\omega_d t_i)\right)^2+\left(\sum_{i=1}^{n}A_i e^{\zeta\omega t_i}\sin(\omega_d t_i)\right)^2} \quad (1)$$

where A_i and t_i are the amplitudes and time locations of the impulses, n is the number of impulses in the input shaper, t_n is the time of the last impulse, and $\omega_d=\omega\sqrt{1-\zeta^2}$.

When Eq. 1 is set equal to zero, it generates two constraint equations because both the cosine and sine terms must equal zero independently for the entire expression to equal zero. When these constraints are combined with the requirements that the impulse amplitudes be positive and sum to one, the two-impulse, Zero Vibration (ZV) shaper shown in Figure 1 can be determined. (The impulses in an input shaper must sum to one so that the shaped command will have the same final setpoint as the unshaped command.) When the ZV shaper is convolved with a step input, the result is a posicast command signal [20].

The ZV input shaper is often not very effective on real systems because it is sensitive to modeling errors and system nonlinearities. To display this result, we plot the shaper's *sensitivity curve*: a plot of vibration versus frequency, (Eq. 1

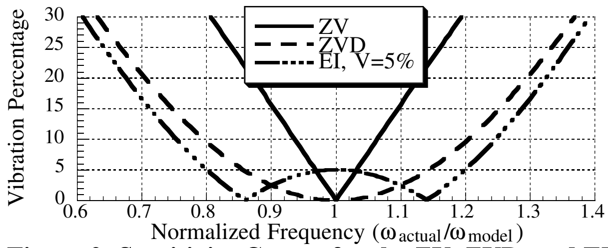

Figure 2: Sensitivity Curves for the ZV, ZVD, and EI Input Shapers.

plotted as a function of ω). Figure 2 shows the sensitivity curve for the ZV shaper. Small deviations from the modeling frequency lead to large amounts of residual vibration.

To make input shaping effective on real systems, equations must be added to the problem formulation to ensure that the vibration will remain at a low level when there is at modeling error. Traditionally this has been accomplished by taking the derivative of Eq. 1 with respect to ω and setting it equal to zero [14]. In equation form:

$$0=\frac{d}{d\omega}(V(\omega)) \tag{2}$$

Solving Eqs. 1 and 2 yields the three-impulse, Zero Vibration and zero Derivative (ZVD) shaper.

Figure 2 shows that the ZVD shaper is much more insensitive to modeling errors than the ZV shaper. However, the ZVD shaper has a time duration equal to one period of the vibration frequency, as opposed to the one-half period length of the ZV shaper. This trade-off is typical of the input shaper design process – increasing insensitivity usually requires increasing the length of the input shaper.

An input shaper with even more insensitivity than the ZVD can be obtained by setting the second derivative of Eq. 1 with respect to ω equal to zero. This shaper is called the ZVDD shaper. The algorithm can be extended indefinitely with repeated differentiation of the percentage vibration equation. For each differentiation, an additional impulse is added to the shaper and the shaper is lengthened by one-half period of the frequency. Closed-form solutions of the ZV, ZVD, and ZVDD shapers for damped systems exist [14].

An alternate procedure for increasing insensitivity uses extra-insensitive (EI) constraints [18]. Instead of forcing the residual vibration to zero at the modeling frequency, the residual vibration is only reduced to a low level, V. The width of the notch in the sensitivity curve is then maximized by forcing the vibration to zero at two frequencies, one lower than the modeling frequency, and the other higher. The sensitivity curve for the EI shaper when V=5% is compared to the ZV and ZVD shapers in Figure 2. The EI shaper achieves the added insensitivity while maintaining the same time duration as the ZVD shaper (one cycle of vibration). The EI shaper for undamped systems is [18]:

$$\begin{array}{lll} A_1=\frac{1+V}{4} & A_2=\frac{1-V}{2} & A_3=\frac{1+V}{4} \\ t_1=0 & t_2=0.5T & t_3=T \end{array} \tag{3}$$

where, T=2π/ω. See [18] for equations that describe the EI shaper as a function of damping ratio. Extending the EI design algorithm to more insensitive, multi-hump shapers is the main purpose of this paper.

Undamped Multi-Hump Extra-Insensitive Input Shapers

The EI shaper for undamped systems presented above contains three-impulses, has a length equal to one period of vibration, and yields a one-hump sensitivity curve. A natural extension would be to design a shaper with two humps in its sensitivity curve, like the one shown in Figure 3. We hypothesize that there exists a shaper containing four evenly

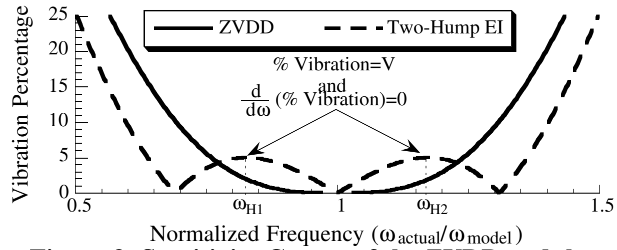

Figure 3: Sensitivity Curves of the ZVDD and the Two-Hump EI Shapers .

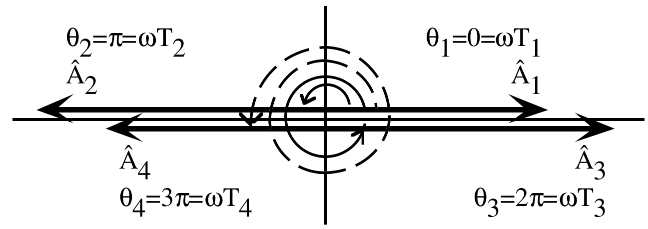

Figure 4: Vector Diagram Representation of the Two-Hump EI Input Shaper.

spaced impulses with a duration of one and a half periods that will form the sensitivity curve of Figure 3.

To simplify the equations in the following derivation, we will transfer the problem of determining the two-hump EI input shaper to a vector diagram. A vector diagram is a graphical representation of an input shaper in polar coordinates. A vector diagram is created by plotting each impulse as a vector with its tail at the origin. The length of the vector is the impulse amplitude, and the angle of the vector is $\theta=\omega t$, where ω is the frequency and t is the time location of impulse. When an input shaper is plotted on a vector diagram, the amplitude of the resultant from summing the vectors is proportional to the residual vibration. To clarify the distinction between impulses and the vectors used to represent them, vectors will be denoted as, $\hat{A}_i$, while impulses and vectors lengths will be denoted as A_i.

A modeling error or frequency shift appears on the vector diagram as a rotation of each vector through an angle $\phi_i=\Delta\omega t_i$, where Δω is the frequency error. Once the vectors have been rotated away from their starting positions, their resultant represents the residual vibration that will occur in the presence of the modeling error represented by Δω. A vector diagram of the proposed two-hump EI shaper is shown in Figure 4. For more details on the vector diagram representation of input shapers see [18] or pp. 54-60 of [13].

By examining Figure 3, we can construct the set of constraint equations that must be satisfied by the shaper in Figure 4. The first requirement suggested by Figure 3 is that the vibration must be zero when the modeling frequency is exactly equal to the actual frequency. This means that the resultant of the vectors shown in Figure 4 must sum to zero when $\Delta\omega=\phi_i=0$:

$$A_1-A_2+A_3-A_4=0 \tag{4}$$

Given that the desired sensitivity curve is symmetrical, the shaper amplitudes must also be symmetrical. This yields:

$$A_1=A_4 \quad \text{and} \quad A_2=A_3 \tag{5-6}$$

Equations 4-6 are not independent; (5) and (4) yield (6). Therefore, (6) is not used in the following derivation.

Figure 3 also indicates that at ω_{H1}, a frequency lower than the modeling frequency, the vibration must equal V and the derivative must equal zero. On the vector diagram these constraints translate to:

$$V=\sqrt{\left(\sum_{i=1}^{4}A_i\cos((i-1)\phi)\right)^2+\left(\sum_{i=1}^{4}A_i\sin((i-1)\phi)\right)^2} \tag{7}$$

and:

$$0=\frac{d}{d\phi}\sqrt{\left(\sum_{i=1}^{4}A_i\cos((i-1)\phi)\right)^2+\left(\sum_{i=1}^{4}A_i\sin((i-1)\phi)\right)^2} \tag{8}$$

where, $\phi=\Delta\omega t_2$, and $\Delta\omega$ is the difference between ω and ω_{H1}. Equations 7 and 8 contain trigonometric terms with arguments of $(i-1)\phi$. This occurs because the first impulse, $\hat{A}_1$, does not rotate in response to a modeling error; it still occurs at time zero ($\theta_1=0$). However, $\hat{A}_2$ rotates ϕ, $\hat{A}_3$ rotates 2ϕ, and $\hat{A}_4$ rotates 3ϕ; each vector $\hat{A}_i$ rotates $(i-1)\phi$.

Finally, the impulse amplitudes must sum to one:

$$\sum_{i=1}^{4}A_i=1 \tag{9}$$

The five equations for the two-hump EI shaper (Eqs. 4, 5, 7-9) contain five unknowns (A_1, A_2, A_3, A_4, ϕ) and one parameter, V. We can solve for the input shaper amplitudes as a function of V. Combining (4), (5), and (9) yields:

$$A_1=(1-A_2)/2 \tag{10}$$

By expanding (7) and (8), combining terms, and using (10), we obtain:

$$\left[3\sin(3\phi)+4\sin(2\phi)-\sin(\phi)\right]A_1^2-2\sin(2\phi)A_1+\frac{\sin(\phi)}{4}=0 \tag{11}$$

$$\begin{aligned}&[4+2\cos(\phi)-4\cos(2\phi)-2\cos(3\phi)]A_1^2\\&\quad+2[\cos(2\phi)-1]A_1+(1-\cos(\phi))/2-V^2=0\end{aligned} \tag{12}$$

Equation 11 can be solved for $\cos(\phi)$:

$$\cos(\phi)=\frac{1}{3}\left(1+\frac{1}{4A_1}\right) \tag{13}$$

Plugging this into (12) yields:

$$A_1=\frac{3X^2+2X+3V^2}{16X}\equiv A_{12H}(V) \tag{14}$$

$$\text{where, } X=\sqrt[3]{V^2\left(\sqrt{1-V^2}+1\right)} \tag{15}$$

Therefore, the two-hump EI shaper for undamped systems is:

$$\begin{array}{llll}A_1=A_{12H}(V) & A_2=\frac{1}{2}-A_1 & A_3=A_2 & A_4=A_1\\ t_1=0 & t_2=0.5T & t_3=T & t_4=1.5T\end{array} \tag{16}$$

Figure 3 compares the two-hump EI shaper to a traditionally designed shaper (a ZVDD shaper) that also has a length of one and one-half periods of vibration.

A three-hump EI shaper can be designed by once again, assuming the shape of the sensitivity curve and establishing constraint equations based on the sensitivity curve. The equations describing the three-hump EI shaper will only be briefly justified because they are very similar to those for the two-hump EI shaper. The amplitude sum constraint is:

$$\sum_{i=1}^{5}A_i=1 \tag{17}$$

Like the one-hump EI shaper, the vibration must equal V when the model is exact, therefore:

$$A_1-A_2+A_3-A_4+A_5=V \tag{18}$$

By symmetry of the sensitivity curve, we get:

$$A_1=A_5 \quad \text{and} \quad A_2=A_4 \tag{19-20}$$

At the first hump of the sensitivity curve, the vibration must be V and the derivative of the vibration expression with respect to ϕ must equal zero. These two constraints yield:

$$V=\sqrt{\left(\sum_{i=1}^{5}A_i\cos((i-1)\phi)\right)^2+\left(\sum_{i=1}^{5}A_i\sin((i-1)\phi)\right)^2} \tag{21}$$

$$0=\frac{d}{d\phi}\sqrt{\left(\sum_{i=1}^{5}A_i\cos((i-1)\phi)\right)^2+\left(\sum_{i=1}^{5}A_i\sin((i-1)\phi)\right)^2} \tag{22}$$

where, once again, ϕ is used to represent the frequency shift (angular rotation on a vector diagram) from the modeling frequency to the frequency corresponding to the first hump in the sensitivity curve.

Combining Eqs. 17-20 we find:

$$A_2=(1-V)/4, \qquad A_3=1-2A_1-(1-V)/2 \tag{23-24}$$

Plugging (23) and (24) into (21) and (22) reduces the problem to two equations with two unknowns (A_1 and ϕ).

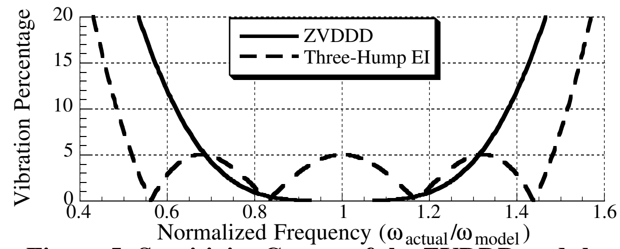

Figure 5: Sensitivity Curves of the ZVDDD and the Three-Hump EI Shapers .

The use of several trigonometric identities and many algebraic manipulations reduces the equations to functions of A_1 and $\cos\phi$ only. These equations are:

$$\begin{aligned}&16\left[1-\cos^2(\phi)\right]\cos(\phi)A_1^2+\left[\left(3\cos^2(\phi)-1\right)(1-V)-2\cos(\phi)(1+V)\right]A_1\\&\quad+\left[\frac{1-V^2}{8}-\frac{(1-V)^2}{8}\cos(\phi)\right]=0\end{aligned} \tag{25}$$

$$\begin{aligned}&4\left(1-\cos^2(\phi)\right)^2A_1^2+2\left(\cos^2(\phi)-1\right)\left[1-\frac{1-V}{2}(1+\cos(\phi))\right]A_1\\&\quad+\frac{1-V}{4}\left[\frac{1-V}{4}\left(\cos^2(\phi)+2\cos(\phi)-3\right)+(1-\cos(\phi))\right]=0\end{aligned} \tag{26}$$

Equation 25 is a cubic in $\cos\phi$. The only real solution is:

$$\cos\phi=(1-V)/(16A_1) \tag{27}$$

Substituting (27) into (26) yields a quartic equation in A_1. Mathematica was used to obtain the four roots. The solution we are seeking is the one that maximizes ϕ (this maximizes the $\Delta\omega$, and therefore, the insensitivity). From (27) we know that we should pick the root that gives the largest value for A_1. This root is:

$$A_1=\frac{1+3V+2\sqrt{2\left(V^2+V\right)}}{16}\equiv A_{13H}(V) \tag{28}$$

Therefore, the undamped three-hump EI shaper is:

$$\begin{array}{lllll}A_1=A_{13H}(V) & A_2=(1-V)/4 & A_3=1-2(A_1+A_2) & A_4=A_2 & A_5=A_1\\ t_1=0 & t_2=0.5T & t_3=T & t_4=1.5T & t_5=2T\end{array} \tag{29}$$

Figure 5 compares the three-hump EI shaper to a traditionally designed shaper (a ZVDDD shaper) that also has a length of two cycles of vibration. Figures 2, 3, and 5 demonstrate that the EI design algorithm produces input shapers that have more insensitivity for a given shaper length than traditionally designed shapers.

Multi-Hump EI Shapers for Damped Systems

The multi-hump EI design procedure can easily be used for damped systems. Three modifications to the above analysis must be performed. First, the damped vibration equation and the derivative of the damped vibration equation must be used in the set of constraints. These equations were given in (1) and (2). Second, the assumption of a symmetrical input shaper must be discarded. The discarded equations are replaced by constraints describing the sensitivity curve on both sides of the modeling frequency. The above undamped procedure only constrained one half of the sensitivity curve, because the symmetry of the input shaper ensured the proper shape for the other half of the sensitivity curve. (Only constraints at ω_{H1} of Figure 3 were used; damping requires that we also form constraint equations for ω_{H2}.) Third, the set of constraint equations must be solved numerically.

We have numerically solved the damped equations for the two and three-hump EI shapers over a range of damping ratios. The amplitudes and time locations of the two-hump EI V=5% shaper and the three-hump EI V=5% shaper are given in Table 1. The curve fits for the two-hump EI shaper have maximum errors in the impulse times and amplitudes of less than 0.5% over the range $0\leq\zeta\leq0.3$. The curve fits for the three-hump EI shaper are accurate to within 0.4% over the range $0\leq\zeta\leq0.2$.

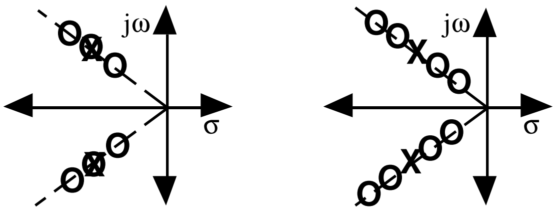

a) Two-Hump EI b) Three-Hump EI

Figure 6: Zero Locations of the Two- and Three-Hump EI Input Shapers in the S-Plane.

Table 1: Damped Multi-Hump EI Shapers

Shaper		$t_i = \left(M_0 + M_1\zeta + M_2\zeta^2 + M_3\zeta^2\right)T, \quad T = 2\pi/\omega$			
		$A_i = M_0 + M_1\zeta + M_2\zeta^2 + M_3\zeta^2$			
		M_0	M_1	M_2	M_3
Two-Hump EI	t_2	0.49890	0.16270	-0.54262	6.16180
	t_3	0.99748	0.18382	-1.58270	8.17120
	t_4	1.49920	-0.09297	-0.28338	1.85710
	A_1	0.16054	0.76699	2.26560	-1.22750
	A_2	0.33911	0.45081	-2.58080	1.73650
	A_3	0.34089	-0.61533	-0.68765	0.42261
	A_4	0.15997	-0.60246	1.00280	-0.93145
Three-Hump EI	t_2	0.49974	0.23834	0.44559	12.4720
	t_3	0.99849	0.29808	-2.36460	23.3990
	t_4	1.49870	0.10306	-2.01390	17.0320
	t_5	1.99960	-0.28231	0.61536	5.40450
	A_1	0.11275	0.76632	3.29160	-1.44380
	A_2	0.23698	0.61164	-2.57850	4.85220
	A_3	0.30008	-0.19062	-2.14560	0.13744
	A_4	0.23775	-0.73297	0.46885	-2.08650
	A_5	0.11244	-0.45439	0.96382	-1.46000

EI Shapers in the S-Plane

We used the time domain and the vector diagram throughout the development of the multi-hump EI shapers. However, a better understanding of the multi-hump EI shapers can be obtained if we examine them in the s-plane.

The zero locations for the multi-hump EI shapers in the s-plane are shown in Figure 6. The two-hump shaper places three zeros near the system pole. One zero is directly on top of the system pole and the others are on either side of the pole along a line of constant damping. If the system model is exact, the first zero completely cancels the pole, leading to zero residual vibration. If the pole moves away from its modeled location due to a modeling error or configuration change, the residual vibration will increase in value until the pole is half way between two zeros. As the pole continues to move away from the modeled location, attenuation of the vibration is dominated by the zero the pole is approaching. If the pole proceeds all the way to one of the outlying zeros, then the vibration will again go to zero. If the pole travels beyond the outer zeros, the vibration will increase steadily.

The three-hump EI shaper places four zeros near the modeling frequency, two on either side along a line of constant damping. This configuration leads to a small amount of residual vibration when the system model is exact. However, it allows the vibration to go to zero at four frequencies near the modeling frequency.

Examining the EI shapers in the s-plane suggests other possible design strategies. Instead of placing the zeros along a line of constant damping, the zeros could be placed at nearby damping values to achieve added insensitivity to errors in the damping ratio. Alternatively, more zeros could be placed on one side of the pole than on the other, or the zeros could be unevenly spaced. These techniques would result in shapers with skewed insensitivity [18].

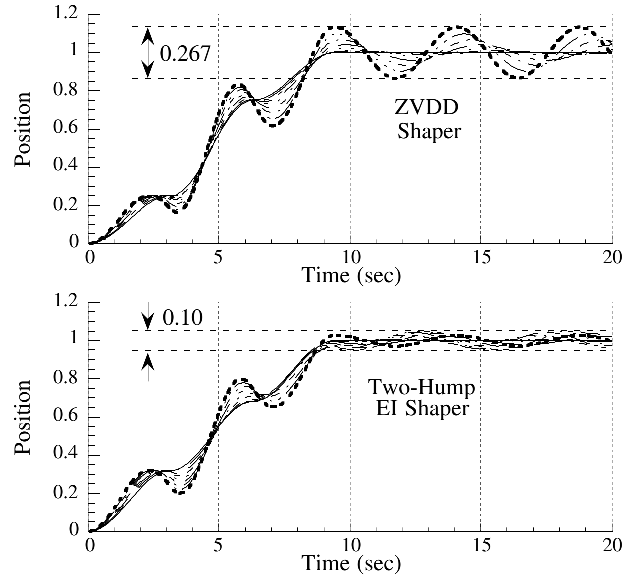

Figure 7 a, b: Responses with the ZVDD & Two-Hump EI Shapers (V=0.05) for $1 \le k \le 1.8$

Simulation Results

Computer simulations were performed using a simple spring-mass system. The nominal mass value, m, and spring constant, k, were both set equal to one. Two-hump and three-hump EI input shapers, with V=5%, were designed for the resulting frequency of $1/(2\pi)$ Hz. The ZVDD and ZVDDD shaper were also designed for the nominal frequency. The system was given step inputs shaped with one of the four input shapers and the position of the mass as a function of time was recorded.

To test the performance of the input shapers in the presence of modeling errors, k was varied from its nominal value of one, and the simulations were conducted again. Figure 7a shows the response of the system with the ZVDD shaped input as k is varied from 1 to 1.8 in steps of 0.1. The envelope containing the residual vibration over this parameter variation has a width of 0.267. Figure 7b shows that the envelope with the two-hump EI shaper over the same parameter variation is approximately 2.7 times smaller (0.10). Even though the two-hump EI and the ZVDD shaper have the same time duration, the two-hump EI bounds the residual vibration to a much lower level.

Figure 8a shows the response of the system with the ZVDDD shaped input as k is varied from 1 to 2.1 in steps of 0.1. A larger parameter variation is shown because the ZVDDD shaper is designed to be more insensitive to modeling errors than the ZVDD shaper. Figure 8b shows that the envelope of the residual vibration is 3.5 times smaller for the same parameter variation when the three-hump EI shaper is used.

The simulation results shown above confirm the important theoretical properties of the multi-hump shapers for use on single-mode systems. The performance of the new shapers on more complicated systems was tested using a multi-mode simulation of the Middeck Active Control Experiment (MACE), which is orbiting the earth in the space shuttle Endeavor as of this writing. MACE is designed to represent a typical satellite with multiple pointing mechanisms. A goal of the experimental program is to develop control algorithms that allow each of the pointing mechanisms to operate accurately in the presence of

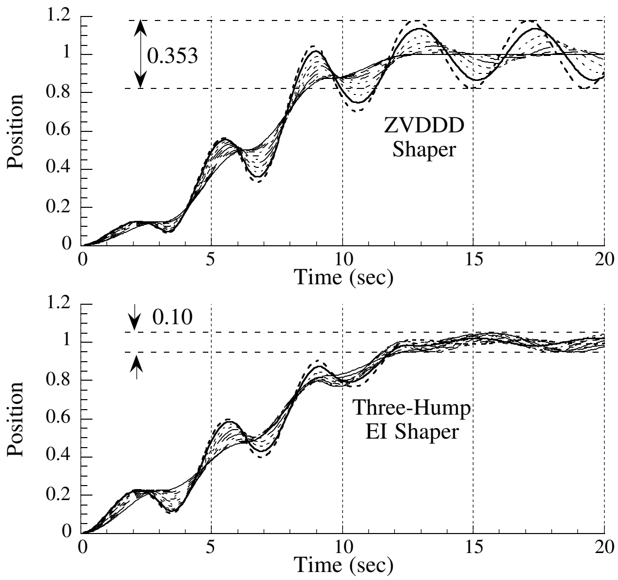

Figure 8 a, b: Responses with the ZVDDD & Three-Hump EI Shapers (V=0.05) for $1 \leq k \leq 2.1$.

disturbances caused by the other pointing mechanism. For more details on the MACE program, see [5, 6, 22].

In one set of scheduled experiments, white noise is fed into the actuator of one of the pointing mechanisms and the response of the other mechanism is recorded. Figure 9 compares the frequency response of the MACE structure without shaping to the case when a two-hump EI shaper is used to modify the command signal. The two-hump notch in the frequency response is readily apparent at the system frequency near 2 Hz.

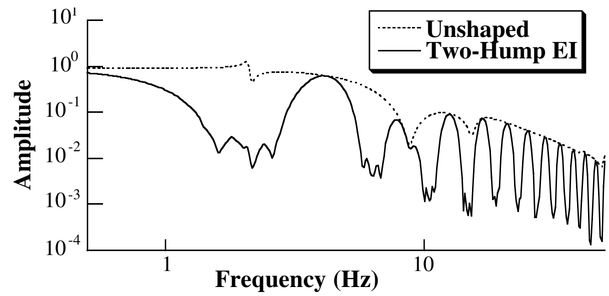

Figure 9: MACE Frequency Response With and Without the Two-Hump EI Shaper.

Conclusions

A procedure for reducing vibration in computer controlled machines has been presented. The procedure utilizes a series of impulses, an input shaper, to modify the command signal. A design method has been developed that generates input shapers that are significantly more insensitive to modeling errors than traditionally designed shapers of comparable duration. Computer simulations of a single-mode system and the multi-mode MACE structure demonstrated the advantages of the new shapers.

Acknowledgments

We would like to thank members of MIT's SERC lab, especially Timothy Tuttle, for help using the MACE simulation. Support for this work was provided by Convolve, Inc. under NASA contract NAS5-32034 and the Office of Naval Research Fellowship Program.

The methods described in this paper are covered under United States patent #4,916,635; April 10,1990, and other patents pending. Commercial use of these methods requires written permission from the Massachusetts Institute of Technology.

References

[1] Banerjee, A. and W. Singhose, "Slewing and Vibration Control of a Nonlinearly Elastic Shuttle Antenna," *AIAA Guidance, Navigation, and Control Conference*, Scottsdale, AZ, 1994.
[2] Bhat, S.P. and D.K. Miu, "Precise Point-to-Point Positioning Control of Flexible Structures," *ASME Journal of Dynamic Systems, Measurement, and Control*, **112**(4): p. 667-674, 1990.
[3] Bolz, R.E. and G.L. Tuve, *CRC Handbook of Tables for Applied Engineering Science*. 1973, Boca Raton, FL: CRC Press, Inc. 1071.
[4] Drapeau, V. and D. Wang, "Verification of a Closed-loop Shaped-input Controller for a Five-bar-linkage Manipulator," *IEEE International Conference on Robotics and Automation*, Atlanta, GA, Vol. 3, pp. 216-221, 1993.
[5] Glaese, R.M., *Development of Zero-Gravity Structural Control Models from Ground Analysis and Experimentation*, Master's Thesis, Massachusetts Institute of Technology, 1994.
[6] Glaese, R.M. and D.W. Miller, "On-Orbit Modelling of the Middeck Active Control Experiment," *12th International Modal Analysis Conference*, Honolulu, Hawaii, 1994.
[7] Jansen, J.F., "Control and Analysis of a Single-Link Flexible Beam with Experimental Verification," *ORNL/TM-12198*, Oak Ridge National Laboratory, 1992.
[8] Jones, S.D., *Quantification and Reduction of Dynamically Induced Errors in Coordinate Measuring Machines*, Ph.D. Thesis, University of Michigan, Ann Arbor, MI, 1993.
[9] Liu, Q. and B. Wie, "Robust Time-Optimal Control of Uncertain Flexible Spacecraft," *Journal of Guidance, Control, and Dynamics*, **15**(3): p. 597-604, 1992.
[10] Magee, D.P. and W.J. Book, "Filtering Schilling Manipulator Commands to Prevent Flexible Structure Vibration," *American Control Conference*, Baltimore, MD, 1994.
[11] Rappole, B.W., N.C. Singer, and W.P. Seering, "Multiple-Mode Impulse Shaping Sequences for Reducing Residual Vibrations," *ASME Mechanisms Conference*, Minneapolis, MN, 1994.
[12] Seth, N., K.S. Rattan, and R.W. Brandstetter, "Vibration Control of a Coordinate Measuring Machine," *IEEE Conference on Control Applications*, Dayton, OH, 1993.
[13] Singer, N.C., "Residual Vibration Reduction in Computer Controlled Machines," *MIT Artificial Intelligence Lab Technical Report No. AITR-1030*, 1989.
[14] Singer, N.C. and W.P. Seering, "Preshaping Command Inputs to Reduce System Vibration," *ASME Journal of Dynamic Systems, Measurement, and Control*, **112**(March): p. 76-82, 1990.
[15] Singh, T. and G.R. Heppler, "Shaped Input Control of a System With Multiple Modes," *ASME Journal of Dynamic Systems, Measurement, and Control*, **115**(September): p. 341-437, 1993.
[16] Singh, T. and S.R. Vadali, "Robust Time-Optimal Control: A Frequency Domain Approach," *Journal of Guidance, Control, and Dynamics*, **17**(2), 1994.
[17] Singhose, W., S. Derezinski, and N. Singer, "Extra-Insensitive Shapers for Controlling Flexible Spacecraft," *AIAA Guidance, Navigation, and Control Conference*, Scottsdale, AZ, 1994.
[18] Singhose, W., W. Seering, and N. Singer, "Residual Vibration Reduction Using Vector Diagrams to Generate Shaped Inputs," *ASME Journal of Mechanical Design*, **116**(June): p. 654-659, 1994.
[19] Singhose, W. and N. Singer, "Initial Investigations into the Effects of Input Shaping on Trajectory Following," *American Control Conference*, Baltimore, MD, 1994.
[20] Smith, O.J.M., *Feedback Control Systems*. 1958, New York: McGraw-Hill Book Company, Inc. pp. 331-345.
[21] Tuttle, T.D. and W.P. Seering, "A Zero-Placement Technique for Designing Shaped Inputs to Suppress Multiple-Mode Vibration," *American Controls Conference*, Baltimore, MD, 1994.
[22] Tuttle, T.D. and W.P. Seering, "Vibration Reduction in 0-g Using Input Shaping on the MIT Middeck Active Control Experiment," *American Control Conference*, Seattle, WA, 1995.
[23] Wie, B., R. Sinha, and Q. Liu, "Robust Time-Optimal Control of Uncertain Structural Dynamic Systems," *Journal of Guidance, Control, and Dynamics*, **15**(5): p. 980-983, 1993.